ADVANCED QUANTUM TECHNOLOGIES
www.advquantumtech.com

Dressing-Shaped Rabi Oscillation of Photon Pairs in Hot Atomic Ensemble

Kangkang Li, Sifan Li, Changbiao Li, Yin Cai, Feng Li, and Yanpeng Zhang**

The nonclassical states of light serve as potential candidates for emerging quantum information processes. A quantum information unit with higher information capacity is interesting and useful in large quantum information systems, such as quantum computations. The most mature way to increase information capacity is to employ a post-selection or cascaded method with the biphoton state and polarizing beam splitters to increase the qubits of the entangled state. Another promising processing is shaping the temporal correlations of entangled state to high-dimensional entangled states to increase the superposed states of each qubit. Based on the photon pair state in a hot atomic ensemble, experiments are conducted to shape its temporal correlations to multi-periodic Rabi oscillations and nonlinear phase shifts. By employing the external dressing field to quantum transitions, the nonlinear interaction produces multiple frequency modes, shaping the temporal correlation of photon pairs to multi-periodic Rabi oscillation and proposing a 3D energy–time-entangled qubit for photon pair state. Interestingly, the maximum peak of the periodic Rabi oscillation can migrate with a longer correlation time because of a nonlinear phase shift. Wave shaping of the photon pair state, therefore, has the potential for applications in quantum information processes with higher information capacity and quantum memory.

1. Introduction

It is well known that photon pairs generated through nonlinear processes provide standards for basic research and potential applications of quantum optics. Based on a two-qubit entangled state, many theoretical and experimental works have made efforts to increase the information capacity of the quantum information unit, which are needed for large quantum information processes. Generally, the most common way to generate photon pairs is by employing spontaneous parameter down-conversion (SPDC),[1,2] in which a strong pump laser drives a nonlinear process and generates two down-converted beams. Based on such entangled photon pairs, termed as biphoton, many proposals have been developed to generate multi-qubit entangled states by the post-selection method with polarizing beam splitters or optical frequency combs to increase its information capacity.[3–5] However, the bandwidth of the photon pairs generated by the SPDC method is broad and can reach the order of terahertz with short coherence times of approximately a few picoseconds.[6,7] Because of these features, most of the existing single-photon detectors (resolution in the nanosecond range) are unable to distinguish the properties of the waveform of such photon pairs. Therefore, many proposals are explored for generating a narrow bandwidth photon pair in the past more than one decade, such as using the optical cavity and passive filtering to narrow down the bandwidth of SPDC photons.[8–13] However, it is still far from the bandwidth of atomic resonance and wider than the bandwidth for most atomic transitions. Besides, the low conversion efficiency in these processes makes it difficult to implement multi-qubit entangled states in an atomic-memory-based quantum network.[12–17]

Subsequently, biphoton state produced from the atomic ensemble with properties such as narrow bandwidths, long coherence times, high spectral brightness, and high conversion efficiency have been investigated both theoretically and experimentally.[6,7,17–34] These optical properties of the new entangled qubits source may have applications in long-distance quantum communication and quantum information processing.[18] In particular, in a hot atomic system, photon pairs were generated with a smaller and simpler apparatus, resulting in lower costs and simpler experimental operations and requirements.[17,26] However, in such a system, a problem is encountered in that uncorrelated photons are generated from the resonance Raman scattering that overwhelms the biphoton. To overcome this problem, Du's team employs a spatially separated optical pumping to suppress the uncorrelated photons, which shows a good performance in reducing the number of accidental coincidence of uncorrelated photons.[17]

Most importantly, with the benefits of long atomic coherence and multiparameter control features in the photon–atom interactions, the temporal correlation of biphoton can be conveniently modulated with the parameters of classical input lasers.[6,7,17–34] Therefore, shaping the temporal correlation with controllable

Dr. K. Li, S. Li, Prof. C. Li, Prof. Y. Cai, Prof. F. Li, Prof. Y. Zhang
Key Laboratory for Physical Electronics and Devices of the Ministry of Education, Shaanxi Key Lab of Information Photonic Technique
Xi'an Jiaotong University
Xi'an 710049, China
E-mail: caiyin@xjtu.edu.cn; ypzhang@mail.xjtu.edu.cn

The ORCID identification number(s) for the author(s) of this article can be found under https://doi.org/10.1002/qute.202000098

DOI: 10.1002/qute.202000098

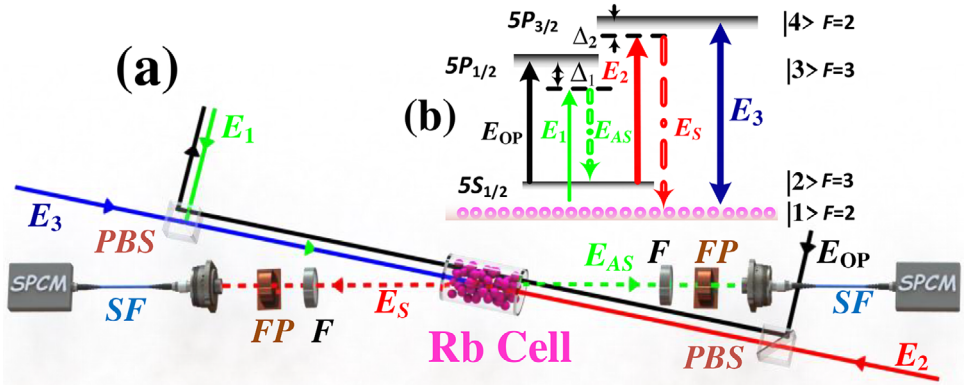

Figure 1. Experimental setup. a) Spatial beam alignment of coexisting biphoton process. F, filter; FP, Fabry–Perot cavity; PBS, polarization beam splitter. b) Energy-level diagram for the four levels configuration in ^{85}Rb vapor.

wave functions of entangled states is particularly interesting in the field of quantum information science and technology. In a three- or four-level atomic system, the biphotons states are investigated theoretically and experimentally by the four-wave mixing (FWM) process with the transparent electromagnetic induction window.[6,7,17–34] Here, the properties of photon pairs can be manipulated by changing the phase-matching function or/and the nonlinear susceptibility.[6,7,17–34] Therefore, the wave function of photon pairs can be shaped for observation of damped Rabi oscillations or Sommerfeld–Brillouin optical precursors, or in between.[6,7,17–34] Furthermore, a type of high-dimensional energy–time-entangled qubit was studied theoretically and proposed to exhibit greater information capacity resulting from shaping the wave packet of photon pairs in an atomic ensemble.[6] In this case, the energy–time-entangled biphoton with multifrequency modes can increase the superposed states of each qubit, which is a novel and effective method to enhance the information capacity of the quantum information unit.[6]

In this article, we report dressing-shaped biphoton Rabi oscillations in a hot ^{85}Rb atomic vapor cell. It is efficient to shape the temporal correlation of the wave packet of biphoton in hot atomic ensembles because of the strong interactions in a photon–atom coupling device. By controlling the biphoton wave shape with different optical depth (OD) or/and the intensity of dressing effect, the Rabi oscillations region and group delay region have been observed in the temporal correlation of biphotons.[6,7,17–34] In the group delay region, the temporal waveform of biphoton with longer coherence time has advantages to encode quantum information. Moreover, in the Rabi oscillation region, the photon pair state can be allowed to shape as high-dimensional energy–time-entangled qubits. In this case, the properties of biphoton temporal correlation, such as oscillation period, frequency modes, coherence time, and nonlinear phase shift, can be shaped by multiparameter control features in atomic vapor system. In a dressed-state picture with the effects of the internal dressing field, the nonlinear susceptibility determines the wave packet of the biphoton as a damped single-period Rabi oscillation. When an external dressing field is applied to the system, the wave packet of biphoton changes from a single period to a multi-periodic oscillation, in which the biphoton waveform confirms the generation of a 3D energy–time-entangled states. Simultaneously, the part oscillation wave peaks can be stored with longer coherence time by multiple features of driving fields, which is resulting from a nonlinear phase shift and delay. Therefore, based on such biphoton state, we experimentally investigated its nonclassical correlation properties in Rabi oscillation region. Moreover, the generated biphotons violate the Cauchy–Schwarz inequality, which shows their nonclassical behavior.[17] These coherent manipulations,[35,36] therefore, are interested and useful in quantum information processes.

2. Experimental Generation of Biphoton

The experimental setup and associated atomic energy-level diagram are illustrated in **Figure 1**. Our experiment was performed in an ^{85}Rb vapor cell at 75 °C. The three lasers, $\boldsymbol{E}_1$, $\boldsymbol{E}_2$, and $\boldsymbol{E}_3$, are employed and pumped by three external cavity diode lasers, respectively. In Figure 1a, the pump laser beam $\boldsymbol{E}_1$ (frequency ω_1, wave vector $\boldsymbol{k}_1$, Ω_1, and horizontal polarization) is employed with a wavelength $\lambda_1 = 794.9780$ nm and detuned by −2.0 GHz from the resonance transition $|1\rangle\rightarrow|3\rangle$, which largely suppresses quantum atomic noise and forces the atomic population to remain in the ground state. Interior dressing coupling laser beam $\boldsymbol{E}_2$ (ω_2, $\boldsymbol{k}_2$, Ω_2, and vertical polarization) drives the transition $|2\rangle\rightarrow|4\rangle$ with $\lambda_2 = 780.237$ nm, and external dressing laser $\boldsymbol{E}_3$ (ω_3, $\boldsymbol{k}_3$, Ω_3, and vertical polarization) drives $|1\rangle\rightarrow|4\rangle$ with $\lambda_3 = 780.230$ nm. The waist of pump and coupling beams at the crossing point is 500 µm, while the waist of external dressing beam is 600 µm. Here, $\Omega_i = \mu_{ij}\boldsymbol{E}_j/\hbar$ is the Rabi frequency with the transition dipole moment μ_{ij}. $\boldsymbol{E}_1$ and $\boldsymbol{E}_2$ generate the phased–matched Stokes ($\boldsymbol{E}_S$, 780 nm, ω_S) and anti-Stokes ($\boldsymbol{E}_{AS}$, 795 nm, ω_{AS}) photon pairs using spontaneous four-wave mixing (SFWM) under phase-matching conditions ($\boldsymbol{k}_1 + \boldsymbol{k}_2 = \boldsymbol{k}_S + \boldsymbol{k}_{AS}$) and energy conservation ($\omega_1 + \omega_2 = \omega_S + \omega_{AS}$); these propagate in opposite directions with a 4° angle along the z-axis such that detecting photons can be distinguished from incident laser beams. The generated photons are coupled through two single-mode optical fibers to linear filters through self-made narrowband etalon Fabry–Perot cavities and are ultimately recorded by single-photon counting modules (SPCM1-SPCM2). A time-to-digit converter with a temporal bin width of 0.0244 ns was used to record the coincidence count of photon pairs. It should be noted that the coupling efficiency of the fiber and the detection efficiency of the SPCM is 70% and 40%, respectively.

The free spectral range one-fourth of the etalon filter is 13.6 GHz. The bandwidth, transmission efficiency, and extinction ratio of the frequency filters are 350 MHz, 80%, and 60 dB for F_{AS} (frequency of Stokes photon), and 80 MHz, 30%, and 40 dB for F_S (frequency of anti-Stokes photon), respectively. To decrease the noise from Raman scattering, an effective forward step of spatially separated optical pumping has been applied in our system.[6] Moreover, the construction involved fiber connections, single-band filters, and homemade narrowband etalon Fabry–Perot cavities to filter most of the noise. Some residuum of uncorrelated single photons and dark counts at SPCMs, which constitutes the background of two-photon coincidence counts, will remain. In hot atomic vapor cells, it is necessary to consider the broadening resulting from the Doppler effect. However, the Doppler effect can only broaden the effective resonance frequencies and mismatching bandwidths but does not change the number of them.[32] Here, we assume that the cell temperature, T, with a very minute deviation and can be viewed as a constant value. Therefore, by applying the Doppler-broadening coefficients, we normalized the optical responses of hot atomic systems and calculated the biphoton coincidence counting rate. The Doppler width is near $\Delta\Omega_D = 551$ MHz; the atomic density is $N = 8.4 \times 10^{11}$ cm^{-3}; L is the rubidium medium length of 7 cm; in this case, we obtain the optical depth $OD = N\sigma_{14}L$ in the hot atomic medium with the value of 46, where $\sigma_{14} = \pi|\mu_{14}|^2/(\varepsilon_0\hbar\lambda_{14}\gamma_{14}\Delta\Omega_D) = 3N\lambda_{14}^2\gamma_{14}L/(8\pi\Delta\Omega_D)$ is the on-resonance absorption cross section in the transition $|1\rangle\rightarrow|4\rangle$; μ_{ij} are the electric dipole matrix elements; λ_{ij} are the resonant transition frequency in the transition $|i\rangle\rightarrow|j\rangle$; γ_{ij} are the dephasing rates of the upper level of the atom; ε_0 is the permittivity of vacuum; and $\hbar$ is the Planck constant divided by 2π.[37,38]

3. Shaping the Biphoton Temporal Correlations in the Photon Coincidence Counting Measurements

The perturbation theory shows that the interaction Hamiltonian can well describe the FWM and determine the evolution of the two-photon state vector.[6,7,17–34] This shows a clear image of the two-photon generation mechanism. The interaction Hamiltonian for our system can be written as

$$\hat{H}_I = \frac{i\hbar}{2}\int d\omega_S d\omega_{AS}\kappa\Phi(\Delta kL)\,\hat{a}_S^{\dagger}(\omega_S)\,\hat{a}_{AS}^{\dagger}(\omega_{AS}) \times e^{-i(\omega_1+\omega_2-\omega_S-\omega_{AS})t} + \text{H.c.} \quad (1)$$

where $\kappa = -i(\sqrt{\varpi_S\varpi_{AS}}/2c)\chi^{(3)}(\omega_S,\omega_{AS})E_1E_2$ is the nonlinear parametric coupling coefficient; ϖ_S and ϖ_{AS} are the central frequencies of the generated photons; $\chi^{(3)}$ is the third-order nonlinear susceptibility of SFWM process; $\Phi(\Delta kL) = \text{sinc}(\Delta kL/2)\exp\{-iL/2[k_S(\omega_S)+k_{AS}(\omega_S)]\}$ is the longitudinal detuning function and determines the natural spectral width; $\Delta\boldsymbol{k} = \boldsymbol{k}_S + \boldsymbol{k}_{AS} - (\boldsymbol{k}_1+\boldsymbol{k}_2)$ is the phase mismatch for the energy configurations employed; $\hat{a}_S^{\dagger}(\omega_S)$ and $\hat{a}_{AS}^{\dagger}(\omega_{AS})$ represent the photon annihilation operators of $\boldsymbol{E}_S$ and $\boldsymbol{E}_{AS}$, respectively; and H.c. is the Hermitian conjugate. According to the first-order perturbation in the interaction picture, we know that the photon state at the output surface is approximately a linear superposition of $|0\rangle$ and $|\Psi\rangle$. We can only consider the two-photon part since vacuum $|0\rangle$ is not detectable. Combined with the quantized fields of generated photons and the frequency entanglement of the biphoton state, the biphoton amplitude (or wave function) in the time domain is given as

$$\Psi(\tau) = \frac{L}{2\pi}\int d\omega_{AS}\kappa(\omega_{AS})\,\Phi(\omega_{AS})\,e^{-i\omega_{AS}\tau} \quad (2)$$

where the relative time delay is defined as $\tau = t_S - t_{AS}$ and L is the length of the rubidium medium. In our experiments, we set the distances between single-photon detectors and the center of vapor cell are also uniform. In this case, the optical path lengths of two fields are same. Here, the relative time delay τ represents the triggering time difference of two single-photon detectors, which is a consequence of the temporal correlation of the biphoton state. In the frequency space, the entanglement is the result of the energy conservation, which implies that detection of the photon frequencies ω_S requiring the detection of the second one at frequency $\omega_1 + \omega_2 - \omega_S$. Therefore, by measuring the two-photon coincidence counting, we can obtain the temporal correlation of the biphoton state.

From the expression for $\psi(\tau)$, we can predict that the biphoton wave function is determined by both the nonlinear coupling coefficient and the longitudinal detuning function.[6,7,17–34] We apply a strong power for coupling field $\boldsymbol{E}_2$, so it is important to consider the strong dressing effect of $\boldsymbol{E}_2$; this could result in the fine-structure-split excited states in a "dressed-state" picture, as shown in **Figure 2**a.[34] If |4> is split, the bare state $\bar{h}\varpi_S$ of photon $\boldsymbol{E}_S$ evolves into double-dressed states $\lambda_{\pm}$ with the bare state $\bar{h}\varpi_S \pm \Omega_{e2}/2$, where $\Omega_{e2} \propto |\Omega_2|^2$ is the efficient Rabi frequency. In this case, the optical properties of $\psi(\tau)$ are mainly determined by the nonlinear coupling coefficient $\kappa(\omega_S)$ and the longitudinal detuning function $\Phi(\Delta kL) \approx 1$. Consequently, by considering 1D Doppler effect only, the corresponding nonlinear susceptibility can be written as

$$\chi_S^{(3)} = \int f(v)\,dv \frac{-N\mu_{13}\mu_{23}\mu_{24}\mu_{14}}{\varepsilon_0\hbar^3(\Delta_{1D}+i\gamma_{31})(w_{D-}\delta+\Delta_{2D}/2-\Omega_{e2}/2+i\gamma_{e2})(w_{D-}\delta+\Delta_{2D}/2+\Omega_{e2}/2+i\gamma_{e2})} \quad (3)$$

Δ_{1D} is the detuning of $\boldsymbol{E}_1$ and is defined as $\Delta_{1D} = \omega_{31} - W_{D-}\omega_1$; Δ_{2D} is the detuning of $\boldsymbol{E}_2$ and is defined as $\Delta_{2D} = \omega_{42} - W_{D+}\omega_2$; W_{D+} W_{D-} are Doppler-broadening coefficients; $W_{D+} = (1 + v/c)$, $W_{D-} = (1 - v/c)$; v is the speed of the atomic motion, and 1D Maxwell–Boltzmann distribution is $f(v) = \sqrt{m_{Rb}/2\pi k_B T}\exp[-m_{Rb}/2k_B T]$;[17] here T is the cell temperature and k_B is the Boltzmann constant, in which the atomic density is estimated from its saturated vapor pressure at the corresponding T with $N = P/(k_B T)$; $\Omega_{e2} = [\Delta_{2D}{}^2 + 4(|\Omega_2|^2 + \gamma_{21}\gamma_{41})]^{1/2}$ is the effective coupling Rabi frequency; $\Omega_2 = \mu_{24}\boldsymbol{E}_2/\bar{h}$ is the coupling-laser Rabi frequency; γ_{41} and γ_{21} are the dephasing rates of coherence $|4\rangle\rightarrow|1\rangle$ and $|2\rangle\rightarrow|1\rangle$, $\gamma_{e2} = (\gamma_{21}+\gamma_{41})/2 + \gamma_{21}\Delta_{2D}/(\Delta_{2D}\pm\Omega_{e2})$ is the effective dephasing rate. We approximate the frequencies ω_S of generated photon as the deviation parameter δ with the corresponding central frequencies ϖ_S. ω_S, then, can be written as $\omega_S = \varpi_S + \delta$. Here, δ represents both the multifrequency nature of biphoton generation and small

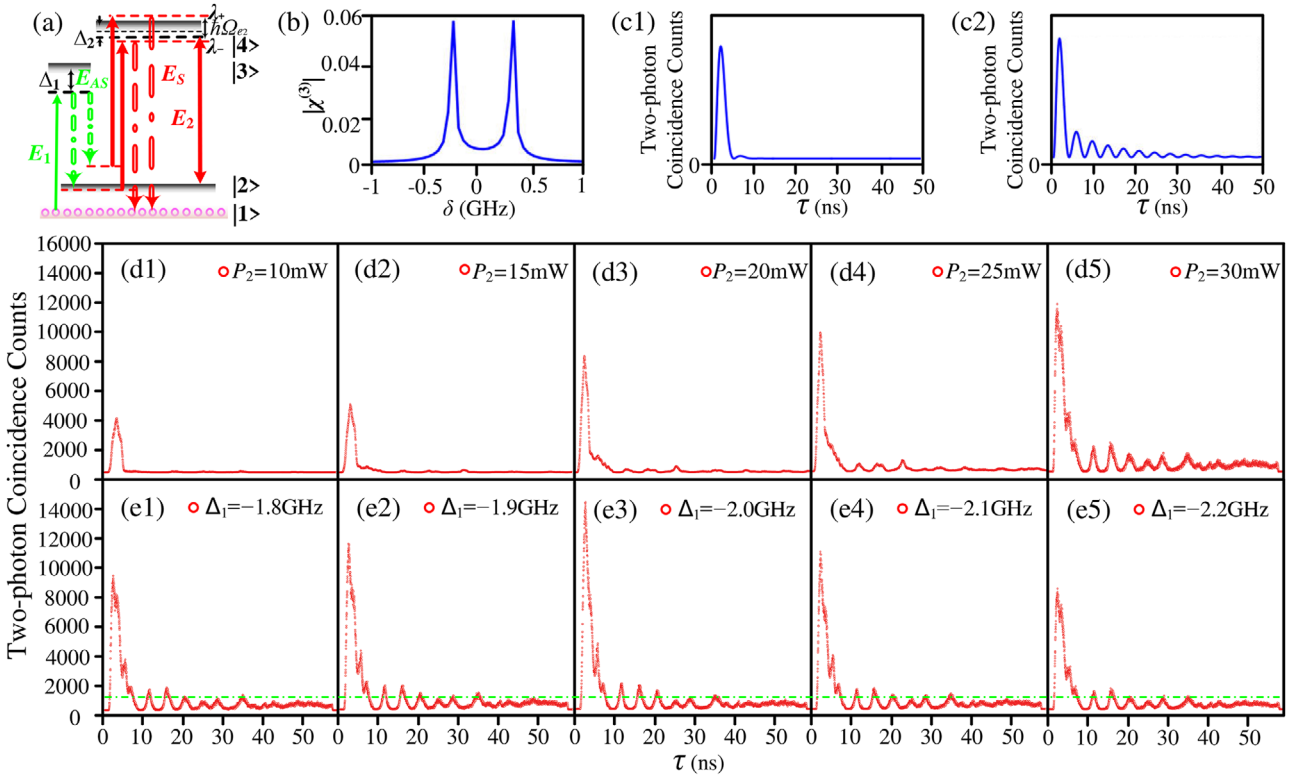

Figure 2. Two-photon coincidence counts. a) The energy-level diagram in the "dressed-state" picture with a strong dressing effect of the coupling field $\boldsymbol{E}_2$. b) The calculated doublet resonances based on the optical resonances of the third-order nonlinear susceptibility $\chi^{(3)}$; $\gamma_{31} = \gamma_{41} = 2\pi \times 3$ MHz; $\Gamma_{11} = \Gamma_{21} = 0.01 \times \Gamma_{31}$; $\Omega_2 = 40 \times \Gamma_{31}$; $\Delta_1 = -106 \times \Gamma_{31}$; $-\Delta_2 = 5 \times \Gamma_{31}$. c) Theoretical simulation pictures of biphoton coincidence counting rate; c1) the parameters are same with (b), but $\Omega_2 = 15 \times \Gamma_{31}$; c2) the parameters are same with (b). d) Two-photon coincidence counting measurements collected over 150 s with 0.02 ns bin width; OD = 43.5, $P_1 = 4$ mW, $\Delta_1 = -2$ GHz, $\Delta_2 = -100$ MHz; d1–d5) with varying power of coupling field $\boldsymbol{E}_2$ as $P_2 = 10$, 15, 20, 25, and 30 mW, respectively; panels (e1–e5) same as (d5), but with varied detuning of the pumping field as −1.8, −1.9, −2.0, −2.1, and −2.2 GHz, respectively.

quantum deviation window located around the corresponding central frequency. On the one hand, with the dressing effect, the variable deviation parameter δ characterizes the Fourier components respect to the doublet or multiple resonant central frequencies in spontaneous emission. On the other hand, in the generated resonant central frequencies or dressed state, the deviation parameter δ results a small quantum deviation window located around the corresponding central frequencies with the limitation of $|\delta| \ll \varpi_S$. Because of the frequency correlation of the biphoton state, the deviation windows for generated photons also satisfy energy conservation and we automatically have $\omega_{AS} = \varpi_{AS} - \delta$. The different quantum properties of the biphoton states can also be reflected by focusing on the photon deviation parameter. The calculated doublet resonances of the third-order nonlinear susceptibility $\chi^{(3)}$ (Equation (2)) are shown in Figure 2b, where each peak represents one of the SFWM coherent channels and dressed states of biophotons. In this case, the photon pair state can be written as a 2D energy–time-entangled state

$$|\Psi_{S,AS}\rangle = N_1|\Psi_{\omega_{AS}+\Omega_{e2}/2,\omega_S-\Omega_{e2}/2}\rangle - N_2|\Psi_{\omega_{AS}-\Omega_{e2}/2,\omega_S+\Omega_{e2}/2}\rangle \quad (4)$$

where N_1 and N_2 satisfy ${N_1}^2 + {N_2}^2 = 1$ and ${N_1}^2 - {N_2}^2 = 0$ because of the normalization and destructive interference.

When the pump field $\boldsymbol{E}_1$ and coupling field $\boldsymbol{E}_2$ are kept constant, the external dressing laser $\boldsymbol{E}_3$ is applied to the quantum transition $|2\rangle \rightarrow |4\rangle$ with a detuning of $\Delta_{3D} = \omega_{14} - W_{D-}\omega_3$ from the atomic transition $|5S_{1/2}, F = 2\rangle \rightarrow |5P_{3/2}, F = 2\rangle$. In this case, the generated dressed-state λ_+ could be split a second time as λ_{++} as shown in **Figure 3**b and the third-order nonlinear susceptibility with the double-dressing effect for the generated Stokes photon can be rewritten as follows

$$\chi_S^{(3)} = \int f(\nu)\, d\nu \frac{-N\mu_{13}\mu_{23}\mu_{24}\mu_{14}}{\left[\begin{array}{c}\varepsilon_0\hbar^3\left(\Delta_{1D}+i\gamma_{31}\right)\left(W_{D-}\delta+\left(\Delta_{2D}-\Omega_{e2}-\Delta_{3D}+\Omega_{e3}\right)/2+i\gamma_{e3}\right)\\ \times\left(W_{D-}\delta+\left(\Delta_{2D}-\Omega_{e2}-\Delta_{3D}-\Omega_{e3}\right)/2+i\gamma_{e3}\right)\left(W_{D-}\delta+\Delta_{2D}/2+\Omega_{e2}/2+i\gamma_{e2}\right)\end{array}\right]} \quad (5)$$

where the dressed effective Rabi frequency Ω_{e3} can written as $\Omega_{e3} = [(\Delta_{2D} - \Omega_{e2} - \Delta_{3D})^2 - {\Delta_{2D}}^2 - 2\Delta_{2D}\Omega_{e2} + |\Omega_{e2}|^2 - 2\Delta_{2D}\Delta_{3D} + 2\Delta_{3D}\Omega_{e2} + 4|\Omega_3|^2 + 4\gamma_{e2}\gamma_{11})]^{1/2}$ and the effective dephasing rate as $\gamma_{e3} = (\gamma_{e2} + \gamma_{11})/2 - [(\gamma_{e2} + \gamma_{11})(\Delta_{2D} - \Omega_{e2})/2 - \gamma_{e2}\Delta_{3D}]/(\Delta_{2D} - \Omega_{e2} - \Delta_{3D} \pm \Omega_{e3})$. The corresponding calculated triple resonances of $\chi^{(3)}$ is shown in Figure 3c. Similarly, the photon pair state can be rewritten as a 3D energy–time-entangled

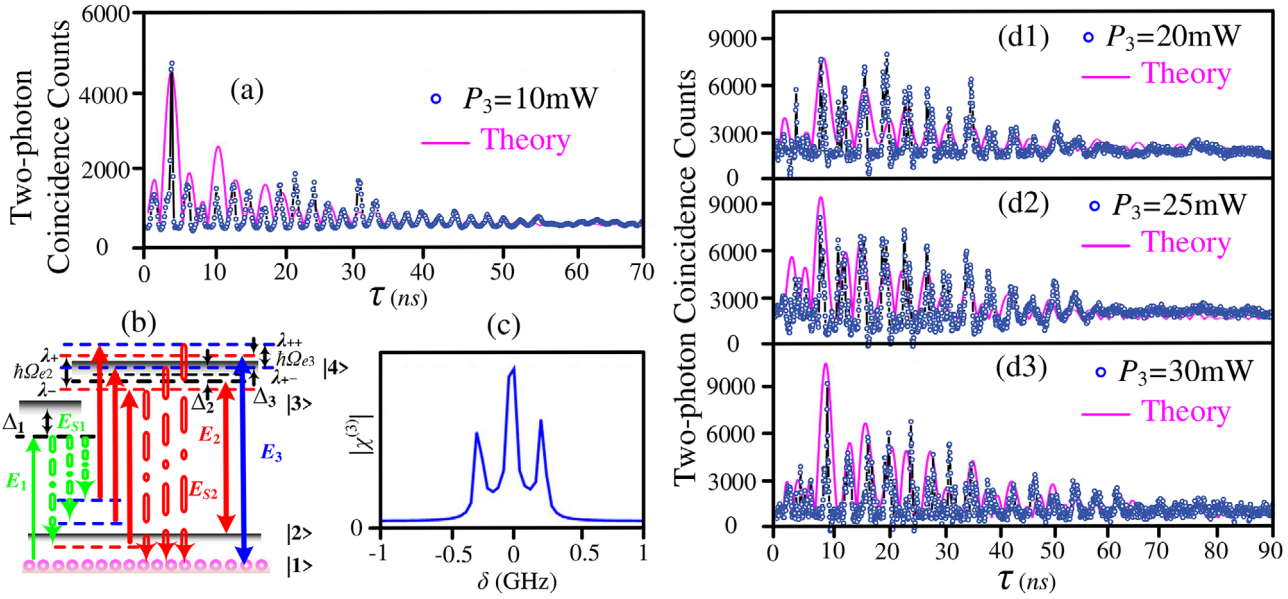

Figure 3. Two-photon coincidence counts. a) Experimental data (-∘- curve) and theoretical simulations (solid curve); the experiment conditions are same as that of Figure 2c5, but with applied an external dressing field $\boldsymbol{E}_3$ and collection time of 60 s; $\Delta_3 = 100$ MHz; $P_2 = 10$ mW. b) The energy-level diagram in the "dressed-state" picture under the double dressing effect of $\boldsymbol{E}_2$ and $\boldsymbol{E}_3$. c) The calculated triple resonances based on $\chi^{(3)}$; $\gamma_{31} = \gamma_{41} = 2\pi \times 3$ MHz; $\Gamma_{11} = \Gamma_{21} = 0.01 \times \Gamma_{31}$; $\Omega_2 = 40 \times \Gamma_{31}$; $\Omega_3 = 40 \times \Gamma_{31}$; $\Delta_1 = -106 \times \Gamma_{31}$; $\Delta_2 = -5 \times \Gamma_{31}$; $\Delta_3 = 5 \times \Gamma_{31}$; panels (d1–d3) are similar to (a), but with the power of dressing field $\boldsymbol{E}_3$ varied as $P_2 = 20$, 25, and 30 mW, respectively.

state

$$|\Psi_{S,AS}\rangle = \left[N_1|\Psi_{\omega_{AS}+\Omega_{e2}/2,\omega_S-\Omega_{e2}/2}\rangle - N_2|\Psi_{\omega_{AS}-\Omega_{e2}/2-\Omega_{e3}/2,\omega_S+\Omega_{e2}/2+\Omega_{e3}/2}\rangle - N_3|\Psi_{\omega_{AS}-\Omega_{e2}/2+\Omega_{e3}/2,\omega_S+\Omega_{e2}/2-\Omega_{e3}/2}\rangle\right] \quad (6)$$

where N_1, N_2, and N_3 satisfy ${N_1}^2 + {N_2}^2 + {N_3}^2 = 1$ and ${N_1}^2 - {N_2}^2 - {N_3}^2 = 0$. In the third-order nonlinear susceptibility in Equation (5), the ratio of resonant intensity of triple resonances can be calculated. Therefore, the normalized coefficients N_i of each dressed state can be fully determined. Based on these three frequency modes of each generated photons, it proposes a 3D frequency-entangled qubit. Therefore, in such 3D energy–time-entangled photon pair state, the information capacity of this quantum information unit can be calculated as 3^2, in which 2 represents the two qubits of this photon pair state and 3 represents the three superposed states corresponding to three frequency modes of each qubit. Moreover, the information capacity of such photon pair state can be extended to n^2 with the n-dimensional energy–time-entangled state by a multi-dressing effect. Therefore, this is an efficient way to increase the number of superposed states of the qubit, thereby enhancing the information capacity of a quantum system.

Ignoring the deviation of the detection, the average biphoton coincidence counting rate is determined by

$$R_{CC}(\tau) = \lim_{T\to\infty} \frac{1}{T} \int_0^T dt_S \int_0^T dt_{AS} \left|\langle 0|E_{AS}^{(+)} E_S^{(+)}|\Psi\rangle\right|^2 \quad (7)$$

where Ψ is the biphoton amplitude; this can be written as $\Psi(\tau) = \psi(\tau) \exp[-i(\omega_1 + \omega_2)t_S]$. Therefore, mathematical calculations allow the biphoton coincidence counting rate of Equation (3) to be expressed as

$$R_{CC}(\tau) = R_0 \left(e^{-2\Gamma_{e2}(\tau - t_\varphi)/W_{D-}} - e^{-2\Gamma_{e2}(\tau - t_\varphi)/W_{D-}} \times \cos\left[\Omega_{e2}(\tau - t_\varphi)/W_{D-} + \Delta\varphi\right]\right)/W_{D-} \quad (8)$$

where R_0 contains all of the constants and slowly varying terms; $\Delta\varphi = \varphi_S - \varphi_{AS} = 2n_2(k_S - k_{AS})e^{-r^2}L/n_1$ represents the relative nonlinear phase shift between Stokes and anti-Stokes signals, which results from cross-phase modulation based on the nonlinear refractive index n_2;[39] φ_S (φ_{AS}) is the nonlinear phase shift induced on the Stokes (anti-Stokes) signal; the parameter r in the formula is the radius of the Gaussian beam incident from the laser, which is equal to the waist of input beams; n_1 is the linear refractive index; n_2 is evaluated from the real component of nonlinear susceptibility as $n_2 = \mathrm{Re}\chi^{(3)}/\varepsilon_0 n_1 c$; and t_φ is the temporal correlation delay from nonlinear phase shift. From Equation (8), the temporal correlation in the biphoton coincidence counting rate may be shown as a periodic Rabi oscillation with a period of $2\pi W_{D-}/\Omega_{e2}$ and decoherence rate of $2\gamma_{e2}/W_{D-}$, which results from the beating and destructive interference between different dressed states of generated photons and coherent energy exchange in different SFWM channels. Here, if the relative nonlinear phase shift is greater than 0, the wave packet could shift far from $\tau = 0$. Besides, different frequency modes of biphoton state have different nonlinear phase shifts and resonance strength in nonlinear susceptibility, which means it can result in different time delay of different frequency modes in same

temporal correlation of biphoton state. Therefore, the dressing effect can shape the biphoton temporal correlation as a periodic Rabi oscillation but also has the effect of a nonlinear phase shift.

Similarly, with the double-dressing effect of Equation (5), the biphoton coincidence counting rate can be calculated, as shown in Equation (9). In this case, the temporal correlation in the biphoton coincidence counting rate is shown as a multi-periodic Rabi oscillation. The oscillation period is roughly $2\pi W_{D-}/\Omega_{e2}$, $2\pi W_{D-}/(\Omega_{e2}+\Omega_{e3}+\Delta_{3D})$, $2\pi W_{D-}/(\Omega_{e2}-\Omega_{e3}+\Delta_{3D})$, and decoherence rates are related to both γ_{e2}/W_{D-} and γ_{e3}/W_{D-}. $\Delta_{\varphi i}$ ($i=1$, 2, 3) are the relative nonlinear phase shifts between Stokes and anti-Stokes photons in different frequency modes. $t_{\varphi i}$ ($i=1$, 2, 3) are the temporal correlation delay from the nonlinear phase shift of each frequency modes. N_i ($i=1$, 2, 3) is the normalized coefficients of each frequency modes, which are determined by the third-order nonlinear susceptibility in Equation (5). In this case, different parameters may manipulate the different temporal properties, such as oscillation periods, nonlinear phase shifts, temporal correlation delay, and the intensity of each frequency mode, of such a 3D energy–time-entangled state

$$R_{CC}=\frac{R_0}{4W_{D-}^2}\times\left[\begin{array}{l}2N_1W_{D-}\Omega_{e3}e^{-\gamma_{e2}(\tau-t_{\varphi1})/W_{D-}}\cos\left[\Omega_{e2}\left(\tau-t_{\varphi1}\right)/2+\Delta\varphi_1\right]\\+N_2\left(\Omega_{e3}-2\Omega_{e2}-\Delta_{3D}\right)e^{-\gamma_{e3}(\tau-t_{\varphi2})/W_{D-}}\\\quad\times\cos\left[\left(\Omega_{e2}+\Omega_{e3}+\Delta_{3D}\right)\left(\tau-t_{\varphi2}\right)/2W_{D-}+\Delta\varphi_2\right]\\+N_3\left(\Omega_{e3}+2\Omega_{e2}+\Delta_{3D}\right)e^{-\gamma_{e3}(\tau-t_{\varphi3})/W_{D-}}\\\quad\times\cos\left[\left(\Omega_{e2}-\Omega_{e3}+\Delta_{3D}\right)\left(\tau-t_{\varphi3}\right)/2W_{D-}+\Delta\varphi_3\right]\\+W_{D-}W_1\end{array}\right]^2 \quad (9)$$

4. Experiment Results of Photon Coincidence Counting Measurements

Figure 2 shows biphoton coincidence counting measurements done in the absence of an external dressing field. Here, the signal detected at SPCM1 serves as the trigger photon, and the signal detected at SPCM2 serves as the stop trigger photon, respectively; we, therefore, recorded the biphoton coincidence counts as shown in Figure 2. In Figure 2d, we observe clear and sharp biphoton coincidence peaks located between $\tau=0$ and $\tau=60$ ns, and each peak represents a strong correlation in this biphoton state. At $\tau=0$, the biphoton coincidence counts rise sharply, whereas at $\tau\to\infty$, they approach zero, and this phenomenon appears as an antibunching-like effect. In Figure 2d1–d5, the power of $\boldsymbol{E}_2$ was increased from 10 to 30 mW. In this case, the Rabi oscillation in the biphoton temporal correlation is more obvious with the enhanced dressing effect of $\boldsymbol{E}_2$. Here, the Rabi oscillation is caused by the beating and destructive interfering between different dressed states of $\hbar\varpi_S\pm\hbar\Omega_{e2}/2$ in Figure 2a,b. The oscillation period and correlation time are ≈4 and 44 ns in Figure 2d5, respectively. The oscillation period can be obtained with the formula $T=2\pi W_{D-}/\Omega_{e2}$ from Equation (8), which is determined by the effective Rabi frequency Ω_{e2}. The damping rate is determined by the inhomogeneous spreading of the ground-state linewidth and the dipole dephasing rate $2\gamma_{e2}/W_{D-}$. With increasing power of $\boldsymbol{E}_2$, the nonlinear susceptibility in Equation (3) is enhanced, which results in increases in the generation of biphoton signals in Figure 2d1–d5. In addition, the signal-to-noise ratios (SNRs) of two-photon wave packets are similar in Figure 2d. Based on the conditions used to generate Figure 2d5, we varied the pumping detuning over the range of −1.8 to −2.2 GHz in Figure 2e1–e5. Here, the pump field $\boldsymbol{E}_1$ is significantly detuned from the resonance, and this is employed to suppress quantum atomic noise and force the atomic population to remain in the ground state. Besides, using the start trigger photon as a fast light is an effective method for increasing the efficiency of the coincidence count measurements. Moreover, based on the corresponding theoretical simulations (solid curve) in Figure 2c1,c2 from Equation (8), they are matching the experimental curves obviously. Further, the near-resonant conditions can also assist the nonlinear process. Therefore, with the increased detuning of $\boldsymbol{E}_1$ seen upon going in Figure 2e1–e3, more biphotons are generated, and SNR increases and reaches a maximum value. The increased SNR could increase the normalized cross-correlation, which reflects a stronger correlation between the Stokes photon and anti-Stokes photon. While pumping detuning increased in Figure 2e4,e5, the biphoton count and SNR decreased gradually because of weak nonlinear susceptibility. To characterize the nonclassical property of the photon pairs source, we confirm its violation of the Cauchy–Schwarz inequality.[17] In Figure 2, the normalized cross-correlation function $g^{(2)}_{S,AS}(\tau)$ of biphoton wave packets reaches its maximum and minimum values of 28 ± 9 and 8 ± 2 in Figure 2d1,e3, respectively. With the autocorrelations of the $\boldsymbol{E}_S$ photon ($g^{(2)}_{S,S}(0)$) and $\boldsymbol{E}_{AS}$ photon ($g^{(2)}_{AS,AS}(0)$), they have a maximum value of 2 and can be measured using a fiber beam splitter. We obtain a violation of the Cauchy–Schwarz inequality $[g^{(2)}_{S,AS}(\tau)]^2/[g^{(2)}_{S,S}(0)g^{(2)}_{AS,AS}(0)]\le1$ by the factors between 51 ± 15 and 16 ± 5 in Figure 2.

Noting the peculiarities of the biphoton temporal correlation in Figure 2, we sought to realize shaping with the external dressing condition. Based on the conditions used to generate Figure 2c5, we applied an external dressing field $\boldsymbol{E}_3$ with power 10 mW (Figure 3a). In this case with the double-dressing effect, the bare state $\hbar\varpi_S$ of photon $\boldsymbol{E}_{AS}$ evolved into three dressed states as $\hbar\varpi_S+\hbar\Omega_{e2}/2\pm\hbar\Omega_{e3}/2$ and $\hbar\varpi_S-\hbar\Omega_{e2}/2$ in Figure 3b,d. These three dressed states are beating and interfere destructively with each other, and the temporal correlation of biphotons in Figure 3a is shown as a multi-periodic Rabi oscillation. Here, two obvious periods of 2.2 and 9 ns are observed. Such multi-periodic Rabi oscillations may also resemble a high-dimensional energy–time-entangled photon pair.[29] Compared with Figure 2c5, the nonlinear susceptibility in Figure 3b is stronger with external dressing field $\boldsymbol{E}_3$, which results in more biphotons and a longer correlation time of 55 ns. In Figure 3d1–d3, we increased the power of $\boldsymbol{E}_3$ from 20 to 30 mW and the multi-periodic Rabi oscillation is more obvious, and the corresponding period becomes complex and changes. Moreover, the theoretical simulations (solid curve) in Figure 3 from Equation (9) are matching the experimental curves obviously. In Figure 3, the calculated factors that violate the Cauchy–Schwarz inequality are between 24 ± 8 and 4 ± 1, which show the nonclassical property of such a high-dimensional energy–time-entangled photon pair state.

Different multi-periodic Rabi oscillations provide different information, which can effectively enhance information capacity. Moreover, another method for shaping the biphoton temporal

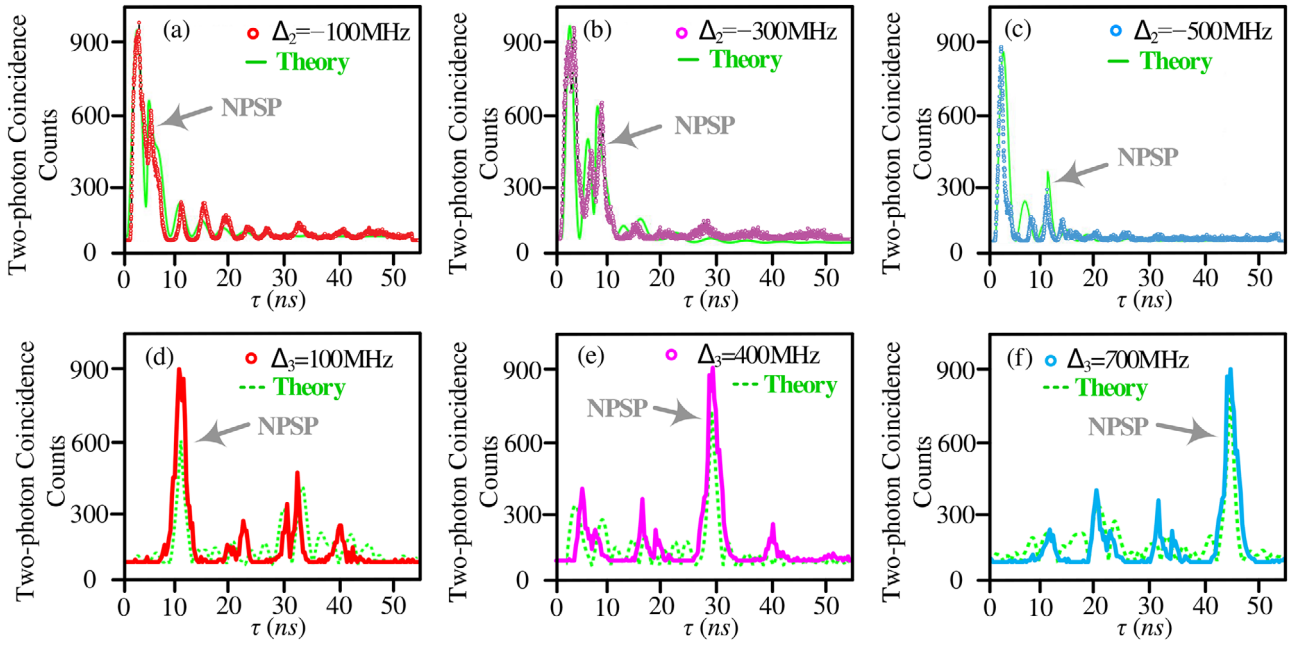

Figure 4. Two-photon coincidence counts for 10 s. a–c) Experimental data (-o- curve) and theoretical simulations (solid curve); the experiment conditions are same as that of Figure 2c5, but with detuning of E_2 varied as −100, −300, and −500 MHz, respectively. d–f) Experimental date (solid curve) and theoretical simulations (dashed curve); the experiment conditions are same as that of Figure 3a, but with the detuning of E_3 varied as 200, 500, and 700 MHz, respectively.

correlation involves applying a nonlinear phase shift. Starting with the conditions used to generate Figure 2d5, we varied the detuning of E_2 by −100, −300, and −500 MHz, as shown in **Figure 4**a–c, respectively. In this case, a nonlinear phase shift peak (NPSP) is separated from the highest wave peak near $\tau \to 0$ and moves far from $\tau = 0$. According to mathematical theory, if the nonlinear phase shift is negative, the peak of the wave position shifts to the right, the nonlinear phase shift $\Delta\varphi$ (Equation (8)) obtained in our case is negative, thus causing the peak position to shift toward the right. Besides, the nonlinear phase shift also results a term of time delay t_φ in Equation (8), which makes the delay of NPSP is more than one Rabi oscillation period. Here, the values of the nonlinear phase shifts in Figure 4a–c are 0, $-\pi/2$, -3π, and -6π, respectively, and the corresponding time delay of NPSP are 5, 10, and 12 ns. In Figure 4a–c, the highest wave peaks are near $\tau \to 0$, which indicates simultaneous situations of $\Delta\varphi = 0$ and $\Delta\varphi \neq 0$. Moreover, the generation of biphotons is decreased, and NPSP is weaker, ongoing in Figure 4a–c, because of the weaker nonlinear susceptibility. Also, the theoretical simulations (solid curve) in Figure 4a–c from Equation (8) are matching the experimental curves obviously. Based on the multi-periodic Rabi oscillation shown in Figure 3a, we varied the detuning of E_2 to 100, 400, and 700 MHz, as shown in Figure 4d–f, respectively. In this case, the values of $\Delta\varphi$ obtained are 0, -4π, and -6π ongoing in Figure 4d–f. The time delay of NPSP is obviously moving from left ($\tau = 11$ ns) to right ($\tau = 45$ ns). NPSPs with long coherence times and delays are useful in quantum memory applications. Besides, in Figure 4d–f, the nonlinear phase shift peak is resulting from the destructive interference between the FWM channel of $\delta = -\Omega_{e2}/2 + \Omega_{e3}/2$ and others two FWM channels of $\delta = \Omega_{e2}/2$ and $\delta = -\Omega_{e2}/2 - \Omega_{e3}/2$. The other small peaks are resulting from the destructive interference between FWM channels of $\delta = \Omega_{e2}/2$ and $\delta = -\Omega_{e2}/2 - \Omega_{e3}/2$ and the residuum part of the mode $\delta = -\Omega_{e2}/2 + \Omega_{e3}/2$, which represent the temporal correlation parts with a weaker nonlinear phase shift. Also, the theoretical simulations (dashed curve) in Figure 4d–f from Equation (9) are matching the experimental curves mainly. Moreover, the calculated factors that violate the Cauchy–Schwarz inequality are near 23 ± 6 in Figure 4. Therefore, the manipulation of the nonlinear phase shift is a novel and effective method for shaping the temporal correlation of the biphoton state.

5. Conclusion

We have investigated the dressing-shaped nonclassical correlated photon pairs generated in hot atomic vapor from SFWM in a four-energy-level system. With the addition of double-dressing fields, the two-photon temporal correlation is shaped as a multi-periodic Rabi oscillation. It is manipulated with the different parameters of the dressing fields. Moreover, different relative nonlinear phases for generated photons based on the nonlinear refractive index result in different nonlinear phase shifts in two-photon temporal correlations, which could delay the correlation wave peak by more than 40 ns. These outcomes provide a new method and platform for generating photon pairs with higher information capacity and quantum memory.

Acknowledgements

This work was supported by the National Key Research and Development Program of China (2017YFA0303700 and 2018YFA0307500) and National

Natural Science Foundation of China (61975159, 61605154, 11604256, 11804267, and 11904279).

Conflict of Interest

The authors declare no conflict of interest.

Keywords

biphoton temporal correlation, energy-time-entangled qubits, nonlinear optics, Rabi oscillations

Received: September 2, 2020
Revised: November 3, 2020
Published online: December 18, 2020

[1] S. E. Harris, M. K. Oshman, R. L. Byer, *Phys. Rev. Lett.* **1967**, *18*, 732.
[2] D. C. Burnham, D. L. Weinberg, *Phys. Rev. Lett.* **1970**, *25*, 84.
[3] J. Pan, M. Daniell, S. Gasparoni, G. Weihs, A. Zeilinger, *Phys. Rev. Lett.* **2001**, *86*, 4435.
[4] X. Yao, T. Wang, P. Xu, H. Lu, G. Pan, X. Bao, C. Peng, C. Lu, Y. Chen, J. Pan, *Nat. Photonics* **2012**, *6*, 225.
[5] Y. Cai, J. Roslund, G. Ferrini, F. Arzani, X. Xu, C. Fabre, N. Treps, *Nat. Commun.* **2017**, *8*, 15645.
[6] D. Zhang, Y. Zhang, X. Li, D. Zhang, L. Chen, C. Li, Y. Zhang, *Phys. Rev. A* **2017**, *96*, 053849.
[7] S. Du, J. Wen, C. Belthangady, *Phys. Rev. A* **2009**, *79*, 043811.
[8] D. V. Strekalov, A. V. Sergienko, D. N. Klyshko, Y. H. Shih, *Phys. Rev. Lett.* **1995**, *74*, 3600.
[9] L. M. Duan, M. D. Lukin, J. I. Cirac, P. Zoller, *Nature* **2001**, *414*, 413.
[10] Z. Y. Ou, Y. J. Lu, *Phys. Rev. Lett.* **1999**, *83*, 2556.
[11] C. E. Kuklewicz, F. N. C. Wong, J. H. Shapiro, *Phys. Rev. Lett.* **2006**, *97*, 223601.
[12] X. H. Bao, Y. Qian, J. Yang, H. Zhang, Z. B. Chen, T. Yang, J. W. Pan, *Phys. Rev. Lett.* **2008**, *101*, 190501.
[13] J. Fekete, D. Rieländer, M. Cristiani, H. de Riedmatten, *Phys. Rev. Lett.* **2013**, *110*, 220502.
[14] M. Förtsch, J. U. Fürst, C. Wittmann, D. Strekalov, A. Aiello, M. V. Chekhova, C. Silberhorn, G. Leuchs, C. Marquardt, *Nat. Commun.* **2013**, *4*, 1818.
[15] G. Schunk, U. Vogl, F. Sedlmeir, D. V. Strekalov, A. Otterpohl, V. Averchenko, H. G. L. Schwefel, G. Leuchs, C. Marquardt, *J. Mod. Opt.* **2016**, *63*, 2058.
[16] H. Zhang, X. M. Jin, J. Yang, H. N. Dai, S. J. Yang, T. M. Zhao, J. Rui, Y. He, X. Jiang, F. Yang, G. S. Pan, Z. S. Yuan, Y. Deng, Z. B. Chen, X. H. Bao, S. Chen, B. Zhao, J. W. Pan, *Nat. Photonics* **2011**, *5*, 628.
[17] C. Shu, P. Chen, T. K. A. Chow, L. Zhu, Y. Xiao, M. M. T. Loy, S. Du, *Nat. Commun.* **2016**, *7*, 12783.
[18] V. Balić, D. A. Braje, P. Kolchin, G. Y. Yin, S. E. Harris, *Phys. Rev. Lett.* **2005**, *94*, 183601.
[19] P. Kolchin, S. Du, C. Belthangady, G. Y. Yin, S. E. Harris, *Phys. Rev. Lett.* **2006**, *97*, 113602.
[20] S. Du, J. M. Wen, M. H. Rubin, G. Y. Yin, *Phys. Rev. Lett.* **2007**, *98*, 053601.
[21] J. Wen, S. Du, Y. Zhang, M. Xiao, M. H. Rubin, *Phys. Rev. A* **2008**, *77*, 033816.
[22] J. Wen, Y. H. Zhai, S. Du, M. Xiao, *Phys. Rev. A* **2010**, *82*, 043814.
[23] S. Yun, J. Wen, P. Xu, M. Xiao, S. N. Zhu, *Phys. Rev. A* **2010**, *82*, 063830.
[24] J. F. Chen, S. Zhang, H. Yan, M. M. T. Loy, G. K. L. Wong, S. Du, *Phys. Rev. Lett.* **2010**, *104*, 183604.
[25] H. Yan, S. Zhang, J. F. Chen, M. M. T. Loy, G. K. L. Wong, S. Du, *Phys. Rev. Lett.* **2011**, *106*, 033601.S.
[26] X. Li, D. Zhang, D. Zhang, L. Hao, H. Chen, Z. Wang, Y. Zhang, *Phys. Rev. A* **2018**, *97*, 97.
[27] S. Zhang, J. F. Chen, C. Liu, S. Zhou, M. M. T. Loy, G. K. L. Wong, S. Du, *Rev. Sci. Instrum.* **2012**, *83*, 721.
[28] Y. Zhang, U. Khadka, B. Anderson, M. Xiao, *Phys. Rev. Lett.* **2009**, *102*, 013601.
[29] S. Du, P. Kolchin, C. Belthangady, G. Y. Yin, S. E. Harris, *Phys. Rev. Lett.* **2008**, *100*, 183603.
[30] J. Wen, S. Du, M. H. Rubin, *Phys. Rev. A* **2007**, *75*, 033809.
[31] D. Wei, J. F. Chen, M. M. T. Loy, G. K. L. Wong, S. Du, *Phys. Rev. Lett.* **2009**, *103*, 093602.
[32] K. Li, Y. Cai, J. Wu, Y. Liu, S. Xiong, Y. Li, Y. Zhang, *Adv. Quantum Technol.* **2020**, *3*, 1900119.
[33] J. Wen, M. H. Rubin, *Phys. Rev. A* **2006**, *74*, 023809.
[34] S. Du, J. Wen, M. H. Rubin, *J. Opt. Soc. Am. B* **2008**, *12*, 98.
[35] Z. Nie, H. Zheng, P. Li, Y. Yang, Y. Zhang, M. Xiao, *Phys. Rev. A* **2008**, *77*, 3195.
[36] Y. Zhang, A. W. Brown, M. Xiao, *Phys. Rev. Lett.* **2007**, *99*, 123603.
[37] H. Wu, M. Xiao, J. Gea-Banacloche, *Phys. Rev. A* **2008**, *78*, 041802(R).
[38] J. Gea-Banacloche, Y. Li, S. Jin, M. Xiao, *Phys. Rev. A* **1995**, *51*, 576.
[39] I. Ahmed, Z. Zhang, F. Wen, D. Zhang, C. Li, R. Wang, Y. Zhang, *Sci. Rep.* **2016**, *6*, 33568.

